Nano World Journal

https://doi.org/10.17756/nwj.2023-s2-033

Research Article

Open Access

Design and Optimization Based on the Finite Element Method of a Cementitious Block as a Sensible Thermal Energy Storage System

Irene Ramón-Álvarez[1*], Ignacio Peralta[2,3,4], Sergio Sánchez-Delgado[5], Manuel Torres-Carrasco[1] and Antonio Caggiano[6]

[1]*University Carlos III of Madrid, Materials Sciences and Engineering Department-IAAB, Avda. Universidad 30, Leganés, Madrid, Spain*

[2]*Institut für Werkstoffe im Bauwesen, TU Darmstadt, Germany*

[3]*Centro de Investigación de Métodos Computacionales, Universidad Nacional del Litoral/Consejo Nacional de Investigaciones Científicas y Técnicas, Argentina*

[4]*Laboratorio de Flujometría, Facultad Regional Santa Fe, Universidad Tecnológica Nacional, Argentina*

[5]*University Carlos III of Madrid, Thermal and Fluids Engineering Department, Avda. Universidad 30, Leganés, Madrid, Spain*

[6]*Dipartimento DICCA, Università degli Studi di Genova, Genova, Italy*

[*]Correspondence to:
Irene Ramón-Álvarez
University Carlos III of Madrid,
Materials Sciences and Engineering
Department-IAAB,
Avda. Universidad 30, Leganés, Madrid, Spain.
E-mail: iramon@ing.uc3m.es

Received: July 25, 2023
Accepted: September 25, 2023
Published: September 28, 2023

Citation: Ramón-Álvarez I, Peralta I, Sánchez-Delgado S, Torres-Carrasco M, Caggiano A. 2023. Design and Optimization Based on the Finite Element Method of a Cementitious Block as a Sensible Thermal Energy Storage System. *NanoWorld J* 9(S2): S188-S194.

Published by United Scientific Group

Abstract

Ordinary Portland concrete nowadays represents a viable and cheap option as a thermal energy storage (TES) medium in concentrated solar power (CSP) technologies. Current TES CSP applications are typically based on molten salt tanks which are very expensive and suffer from high corrosion problems. Contrarily, concrete presents series of pro such as: simplicity, quite good sensible TES, high availability, easy fabrication, good mechanical properties (even after the exposure to high temperature), and finally, a thermal expansion coefficient near to that of steel, minimizing problems related to the interface between the cementitious material and the heat exchangers (commonly made of steel). In this context, a correct design of the TES medium, composed of the cementitious material (Cementitious materials are nanoscale materials) and the heat exchangers (pipes), plays a key role in both the performance impact as well as on the overall costs of the CSP device. Therefore, it is necessary to optimize TES systems by varying all variables providing the best performance: i.e., number of tubes, their arrangement in the block, as well as the correct selection of the employed cement-based material. To achieve an optimized configuration and design, a finite-element-based approach is implemented for simulation purposes. In these simulations, the number of pipes and their arrangement were varied and, in addition, different alternative mortars to ordinary Portland cement were manufactured and used as input parameters. The alternatives prove to be more efficient than TES as. They reduce the volume of the molten salt tank by 17% and the surface area of the heat exchanger by 29% (high-cost savings) compared to the PC (Portland cement) reference system.

Keywords

Finite element method, Cementitious block, Optimization, Thermal energy storage

Introduction

The lack of competitiveness shown by CSP plants, because of their high economic impact, makes it necessary to find new solutions to minimize (construction and/or maintenance) costs.

To increase the encourage of the CSP as a renewable energy, not only in the electricity generation sector, but also in the industry demand of heat for processes, the TES is a relevant key to explore, improve and optimize. There are many different options to storage the solar energy: sensible energy storage, latent

energy storage or thermochemical energy storage, being the sensible energy storage the most extended technology in the industry due to their easy and cheap operation, however, this technology is not free of uncertainty and challenges to be solved. Nowadays, in the CSP plants for electricity production, the TES is made by sensible energy storage via metal tanks which are filled up with molten salts. To prevent corrosion from molten nitrates, tanks are made of expensive materials such as Ni-based superalloys or austenitic stainless steel. However, corrosion is still an open issue in the field, compromising the safety of the plants within 30 years [1]. Thus, it is interesting to find new solutions to boost CSP plants that can improve their operational aspects and save costs. The sensible storage is the simplest way [2, 3], in where concrete is found to be a viable TES system [4, 5]. In Laing et al. [5], it was proven that concrete can be exposed to thermal cycles, from 200 °C to 400 °C (typical operational temperatures used in the most common CSP technology as parabolic trough collectors, thus concluding that it can operate on a commercial scale. In CSP systems, concrete undergoes repeated cycles of heating and cooling with the use of the energy provided by the heat transfer fluid flowing through embedded steel pipes (heat exchangers), which transfers and/or absorbs heat as it moves through the block. The heat exchangers have the greatest impact on the economy [6], as they can reach more than 50% of the cost of the TES [7], so it is important to optimize the transfer area of the TES to reduce costs. Costs can be reduced by enhancing the block's performance through optimizing its geometry and incorporating multiple pipes into the TES device [8, 9], to optimize the transfer area. This process should always consider the proper choice of pipe diameter, number of pipes and their arrangement in the block to get the maximum transfer of energy: heat exchangers have a greatly influence in charging/discharging times, without neglecting the economic impact [6, 10].

Another way to save costs, in addition to the heat exchanger optimization, is to reduce the TES installation space by getting a block material that can store more energy [11] per volume unit. Recent studies have demonstrated the good performance (from a mechanical, thermal, and environmental point of view) of alternative cementitious materials for use as TES [12, 13]. Particularly, alkali-activated materials (AAM) and hybrid materials (HM) were developed, to cut-back the high environmental impact produced by the main raw material of the concrete: PC. PC negatively impacts the environment due to its high consumption of fossil fuels: e.g., it is responsible of 12 - 15% of the total industrial energy consumption [14] and emits different polluting gases, among them 7 - 9% of the CO_2 global emissions [15]. To minimize those problems, AAM can fully substitute PC using aluminosilicates which are activated with high pH alkaline solutions, that limit the workability in the construction sector [16]. To avoid these types of activators, HM emerged, which substitute partially PC as these materials are used in a low content (20 - 30%) and the aluminosilicate material is now activated with soft alkaline salts just in presence of water [17]. Aluminosilicate materials can come from a natural resource or be waste from other industries (by-products) [12]. By-products can be used as a part of the binder but also, in substitutions of aggregate and sands, to avoid abiotic depletion, eutrophication, acidification [18] and CO_2 emissions [19] among other environmental problems.

In view of the above, this study proposes the development of new alternative mortars as TES systems in CSP plants. For this purpose, the mechanical and thermal properties of the materials were studied after the exposure to 20 thermal cycles (between 200 °C and 400 °C and vice versa). With this characterization, a finite element model (FEM) has been implemented to study which mortar offers a better thermal performance (rapid heat-up and prolonged discharge) in a CSP plant by previously optimizing the geometry of the block and modifying the parameters of the heat exchanger.

Experimentation

Characterization methods

Three mortars were manufactured: a reference mix (labelled as PC) composed of PC; an AAM (SLAG) composed of blast furnace slag that was activated with a commercial sodium silicate (SiO_2/Na_2O = 0.8); and a HM referred as HSLAG, composed of 77.5% of blast furnace slag, 17.5% of PC, and a soft alkaline activator, Na_2SO_4, that was added by 5% to accelerate the hydration process [20]. To reduce the water footprint [21], the natural aggregate (sand) was substituted by glass waste (GW). Mortars were cured for 28 days in a humid climate container (99% relative humidity) at room temperature (22 °C). Then, to study the viability of the materials as TES, thermal cycles were performed between 200 °C and 400 °C, since these are the optimum temperatures at which concrete can operate [22] and because CSP technology usually operates between 290 °C and 390 °C [10]. Heating/cooling ramps of 6 °C/min to ensure high thermal stress were used [23]. To analyze the untreated samples and the ones exposed to 20 cycles, compression tests were carried out (five samples of 4 x 4 x 16 cm for each type of mortar) to study the mechanical properties by using Microtest universal testing machine, with 200 kN load cell to register the necessary force to cause the failure of the mortar. Density was also measured (three repetitions), being an input in the simulation and to calculate the porosity of the samples, as this property affects both mechanical and thermal values. ACCUPYC 1330 helium pycnometer with gas displacement (Micromeritics, Norcross, GA, USA) was used to determine the theoretical density (ρ_t). Bulk density (ρ_b) was calculated by Archimedes principle (see UNE-EN 993-1:2018 standard). With both densities, total porosities (π_t) were calculated. To also solve the heat transfer problem within the mortar, thermal conductivity and specific heat of the materials were measured by using MP-2 Thermal Conductivity Measurement Platform (with the TLS 50 mm sensor – ten measurements) and differential scanning calorimeter (equipment model 822, Mettler Toledo GmbH, Greifensee, Switzerland) (three repetitions per mortar), respectively.

Finite element model

FEM simulations were performed in MATLAB R2021a to study the heating/cooling processes of the blocks during

thermal cycles. To simplify the geometry, the minimum symmetrical portion (unit cell) of the block was modeled. This cell is taken out from a 3 x 3 x 21 m^3 mortar block. Three typical configurations of a heat exchanger [24] were represented (Figure 1) to find out which distribution allows an increase of the operational temperatures to improve the system efficiency and achieve higher sensible heat storage [11]. The block operates adiabatically and is heated by a HTF that flows within the pipes at a charging temperature of 390 °C during 7.5 h. The problem is simplified by assuming that the wall of the pipe is at 390 °C (no internal fluid interactions are considered). For the discharging phase (7.5 h), the temperature of the pipe is 290 °C. To achieve reliable results, the mesh was optimized by dividing the unit cell into 100 elements (10,000 squares generate the mesh). The optimization was carried out based on previous studies [12].

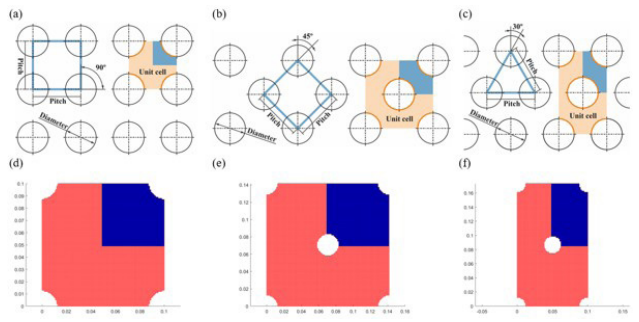

Figure 1: (a), **(b)**, and **(c)** Unit cell arrangements with their main parameters. **(d)**, **(e)**, and **(f)** Geometry and considered mesh studied in the simulation: (**a** and **d**) Square arrangement with a 90° angle; (**b** and **e**) Triangular distribution with an angle of 45°; (**c** and **f**) Triangular distribution with an angle of 30°. The blue area represents the points that provide the average temperature of the quarter of the block.

Basic equations and assumptions

The heat transfer problem considers a conduction-only phenomenon, solved by equation (Eq. 1).

$$\rho_c c_c \frac{\partial T}{\partial t} - \nabla.\left(k\nabla\left(T\right)\right) = q_c\left(T\right) \quad (1)$$

Being k the thermal conductivity and $\nabla \cdot$ and ∇ the divergence and gradient operators, respectively. The temperature field T is discretized in the FE domain assuming interpolation strategy (Eq. 2).

$$T = N.\hat{T} \rightarrow \nabla\left(T\right) = \nabla\left(N.\hat{T}\right) \quad (2)$$

Where $N=[h_1,h_2,...,h_n]$ is the vector collecting the shape functions, while $\hat{T}=\left[\hat{T}_1,\hat{T}_2,...,\hat{T}_n\right]^t$ the nodal temperatures of the iso-parametric FE having n nodes. The first derivative with respect to time t of Eq. (2) can be expressed as (Eq. 3):

$$\frac{dT}{dt} = \mathrm{N}.\frac{d\hat{T}}{dt} = \mathrm{N}.\dot{\mathrm{T}}. \quad (3)$$

Then, Eq. (4) in the FE domain is used to analyze the heat transfer problem:

$$\mathrm{C}^e.\dot{\mathrm{T}} + \mathrm{K}^e.\hat{\mathrm{T}} = \mathrm{F}_Q^e + \mathrm{F}_q^e \quad (4)$$

Where,

$C^e = \int_\Omega N^t \rho_c c_c N d\Omega$ (Capacity matrix operator),

$\mathrm{K}^e = \int_\Omega \nabla \mathrm{N}^t k \nabla \mathrm{N} d\Omega$ (Conductivity matrix operator),

$\mathrm{F}_Q^e = \int_\Omega \mathrm{N}^t \mathrm{Q}_v \, d\Omega$ (Heat load due to heat sources), and

$\mathrm{F}_q^e = \int_{\Gamma n} \mathrm{N}^t \mathrm{q}_n d\Gamma_n$ (Heat load due to heat flow).

Where, Q_v is the rate of heat source and q_n the heat flow, while the boundary surface (Neumann or natural) conditions of the considered FE is denoted by Γn having a volume Ω. By using the classical assembling procedures for the FE analyses in structural problems, Eq. (5) can be obtained.

$$\mathrm{C}\,.\,\dot{\mathrm{T}} + \mathrm{K}\,.\,\mathrm{T} = \mathrm{F}_Q + \mathrm{F}_q \quad (5)$$

Where, C and K are the global constitutive matrices, while F_Q and F_q the assembled global vectors whose values are zero (no heat sources are considered). Then, T is the vector of the nodal temperatures on the global reference system. Finally, for the integration in time of Eq. (5), recourse is made of a Backward-Euler (implicit) time stepping characterized by unconditional convergence.

Results and Discussion

Mechanical properties characterization

After replacing the sand with GW in different percentages, compression tests were carried out. The results show that the introduction of GW decreases the mechanical properties due to the weak bonding between the binder and the aggregate [25] and because GW demands a higher liquid/solid (L/S) ratio which generates more porosity [26]. After those tests, the mortars with the best performance were selected: the three basic systems (PC 100S, SLAG 100S, and HSLAG 100S) and the AAM mortar with a 25% wt. of GW (SLAG 75S). The AAM system was the only one that allowed the introduction of GW without affecting the strength of the material too much (SLAG75 shows a resistance equal to that of the reference PC sample). This is produced thanks to the high cohesion and compaction of the main reaction product (C-A-S-H gel because slag is used) that is produced when silicon is added using sodium silicate [27, 28].

Specifically, as shown in figure 2, the basic AAM mortar (SLAG 100S) without any thermal treatment (WT) reaches a compressive strength value up to 67 MPa, which is an improvement over the reference mortar PC 100 S of 64%. Continuing to focus on the systems without temperature exposure, although the GW reduces the mechanical properties, the SLAG 75S mortar achieves a strength value of 41 MPa which is equal to that obtained in the reference PC system without GW (PC 100S). In the case of the HSLAG 100S, a reduction of only 13% compared to the PC 100S mortar is achieved, reaching a compressive strength value of 35 MPa. This lowest value is due to its main reaction products, which are a mixture of C-S-H gel (produced by the amount of PC

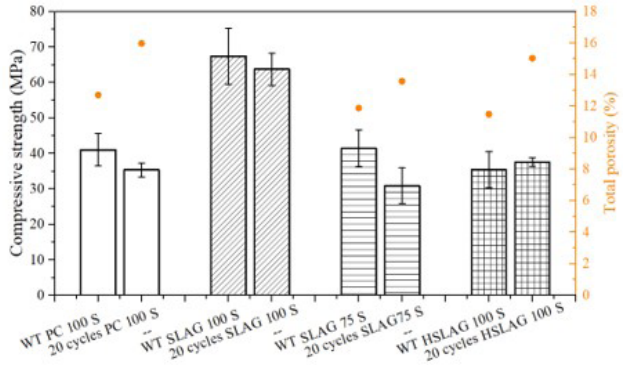

Figure 2: Compressive strength and total porosity of selected systems before thermal treatment and after exposure to 20 thermal cycles.

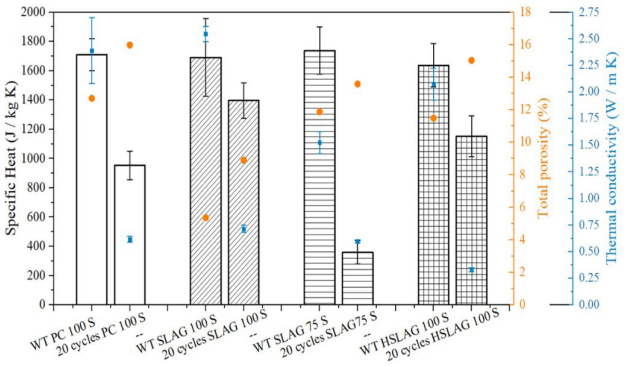

Figure 3: Specific heat, thermal conductivity, and total porosity values of mortars without thermal treatment and after exposure to 20 thermal cycles.

(17.5%)) and a C-A-S-H gel (produced by the 77.5% wt. of slag in the composition). The mixture of gels is not as consistent as the C-S-H gel present in the PC 100S mortar, this is due to the percentages of PC used: 100% of PC in the reference versus 17.5% employed in the HSLAG 100S. Moreover, the C-A-S-H gel of the hybrid system is less cohesive than that of the AAM, since no silica-rich solution is added.

Then, to test the thermal stability of mortars as TES systems, their compressive strength was measured after their exposure to 20 thermal cycles between 200 °C and 400 °C. As can be seen in figure 2, SLAG 100S shows a constant behavior after thermal stress, decreasing its mechanical resistance by only 5% due to the C-A-S-H gel. On the contrary, SLAG 75S suffers the most, with a 25% reduction, due to the weak bond between aggregate and binder caused by incompatibility [29], and the continuous expansion of the aggregate during heating (while the binder shrinks [30]) causes further damage to this system. The second largest reduction comes from the PC 100S, with a drop of 13%. The C-S-H produced in the reference sample is not as cohesive as the C-A-S-H gel of the SLAG 100S. HSLAG 100S, on the other hand, improves its mechanical behavior by 6% after 20 cycles because its exposure to temperature causes reactivity in the material that provides a 6% improvement over PC 100S after 20 cycles. Hydration of HSLAG 100 S with water and with a very small percentage of activator (only 5%), leads to low mechanical performance after 28 days of curing, however, heat treatments have been shown to accelerate the reactivity in the material generating new reaction products that add consistency [31].

The decrease in mechanical properties is related to porosity and cracks produced due to shrinkage after the thermal treatment [32]. Excluding the HSLAG 100S, which is influenced by the equilibrium between the reaction and the formation of the main hydration products mentioned before, it can be seen how porosity increases after thermal cycles and how mechanical properties in the systems decrease.

Thermal properties characterization

After thermal cycles, the thermal properties are also affected. Specifically, thermal conductivity depends mainly on the porosity so, after the temperature exposure, there is a decrease in the thermal conductivity values. Without treatment (WT in figure 3), PC 100S and SLAG 100S show the highest thermal conductivity values. Due to the incompatibility between the binder and the aggregates, SLAG 75S has a thermal conductivity 36% lower than the reference sample. Regarding the HSLAG 100S, the lower consistency of its main reaction products leads to a 13% lower thermal conductivity value in comparison to PC 100S. When samples are exposed to thermal cycles, there is a 16% of improvement in the thermal conductivity of the SLAG 100S over the PC 100S, while SLAG 75S reduces its thermal conductivity (compared to the PC 100S) by only 3%. Compared to the untreated systems, SLAG 100S is affected by 71%, SLAG 75S decreases compared to its untreated sample by 60%, PC 100S by 74% and HSLAG 100S by 84%. These reductions again demonstrate the higher cohesiveness of the C-A-S-H gel compared to the C-S-H gel.

Specific heat is also important to stress as it determines the amount of energy that can be stored in a block together with the mass of the material and the operating temperatures. Stored energy is also affected after thermal cycling due to mass losses (evaporation of water, mass loss of the aggregates [5], decomposition of the gels and components [29]). After thermal cycles, SLAG 75S reduces its capacity (from its untreated sample) by 79% due to the aggregate expansion and the binder shrinkage [30], and due also to the weak bond between the aggregate and the binder caused by incompatibility [29]. The next most affected material is the PC 100S with a reduction compared to its untreated sample of about 44%. Next, HSLAG 100S was affected by about 29% and SLAG 100S by only 17%. Compared to the PC 100S system after the exposure to 20 cycles, it should be noted that there is an improvement in the thermal storage capacity of more than 46%, if the SLAG 100S is used, and of almost 21% if the HSLAG 100S is considered. As seen in the mechanical properties section, thermal stress has a greater impact on the PC 100S system. This demonstrates again the possibility of using alternative materials like TES in the CSP plants.

Finite element simulations

As can be seen in figure 1, the parameters that were varied in the simulation were:

- Pipe distribution: Triangular arrangements with angles of 30° and 45° between the center of the pipes, and square arrangement with an angle of 90°.

- Pipe diameter: Two typical exchanger diameters were used (12.7 and 25.4 mm).
- Number of pipes: The tubes were arranged in a 2-dimensional section of 3 x 3 m^2. The section contains the maximum number of pipes according to the pitch.
- Pitch: Pipe center distance of 70, 80, 90, 100, 110, 120, 130, 134, 140, 150, 200, 300, and 400 mm.

It was first analysed which distribution provided the fastest heating by keeping the pitch and diameter constant. The results show that the triangular distribution with an angle of 30° offers greater system dynamics. Then, using this distribution, the pitch and the outer diameters were varied as described previously. The chosen geometry configurations were those which, for a load of 290 °C to 390 °C during 7.5 h of storage, heat up to at least 380 °C (10 °C below the load temperature) and their total volume to store at least 1100 MWh (capacity for a 50 MWh parabolic trough power plant of the ANDASOL-type [5]) is at most 30% higher than the current volume of common Solar Salt (16011 m^3).

Since the minimum volume required by the SLAG 75S to store 1100 MWh is 230% higher than that of the Solar Salt, this system was rejected. In contrast, the SLAG 100S mortar is the only one that provides a smaller volume than the Solar Salt (Figure 4a) as it can save more than 17% of volume when using an outer diameter of 12.7 mm and a pitch of 80 mm. In the PC 100S system, even if the smaller volume configuration (diameter 12.7 mm and pitch 90 mm) is used, the salt volume is still exceeded by 22%. Although the use of HSLAG 100S increases the volume, choosing the distribution with diameter 12.7 and pitch 70, there is only an increase in volume compared to Solar Salt of more than 1%. So, comparing the minimum volume of cementitious materials with the PC 100S mortar, SLAG 100S provides a volume decrease of 32%, while HSLAG 100S of almost 17%.

In addition to the TES volume, it is important to consider the surface area of the heat exchanger, as these embedded metal tubes account for more than 50% of the total TES price [7]. As figure 4b demonstrated, the diameter reduction (25.4 to 12.7 mm) leads to large material savings. Among all the systems, the only configuration that considers a total area under 100000 m^2 is the SLAG 100S with a pitch of 110 mm and a diameter of 12.7 mm. This result compared to the PC 100S system, which has the smallest tube surface (D = 12.7 mm, Pitch = 110 mm), offers almost 29% material savings. Even when the pitch was reduced to 100 mm in the SLAG 100S, compared to the PC 100S with the smaller tube surface, savings of almost 21% are achieved and the SLAG 100S block heats up after 7.5 h by about 1% more. Further, reducing the pitch to 90 mm, in the AAM system, results in a decrease in the total tube area compared to the PC 100S with minimum tube surface of almost 1% and in a higher heating of the block (3% more) after 7.5 h. For the HSLAG 100 S system, the minimum tube surface is also achieved with a diameter of 12.7 mm but with a pitch of 90 mm. This option, compared to the PC 100S, increases the minimum surface area less than 30%. These results prove once again the feasibility of using alternative materials to PC as TES.

Conclusions

After the experimental and the computational studies, the following concluding remarks can be itemized:

- Regarding mechanical performance, thanks to the high cohesion of the C-A-S-H gel the AAM systems present better mechanical properties. In particular, SLAG 100S system keeps almost constant its strength after the exposure to 20 thermal cycles between 200 °C and 400 °C, providing an 80% improvement compared to the PC 100S. In the case of the HSLAG 100S, it improves its compressive strength over the PC 100S by 6%.
- Porosity must be taken into account if a material is going to be used as a TES medium, as it has influence in both mechanical and thermal properties. Air cavities cause detriment in both aspects.
- Alternative systems offer similar thermal conductivity values to PC 100S. Moreover, the SLAG 100S system improves the thermal conductivity after exposure by 16% compared to PC 100S.
- SLAG 100S and HSLAG 100S systems improve the energy storage capacity compared to that of PC 100S by more than 46% and around 21%, respectively, after thermal cycles.

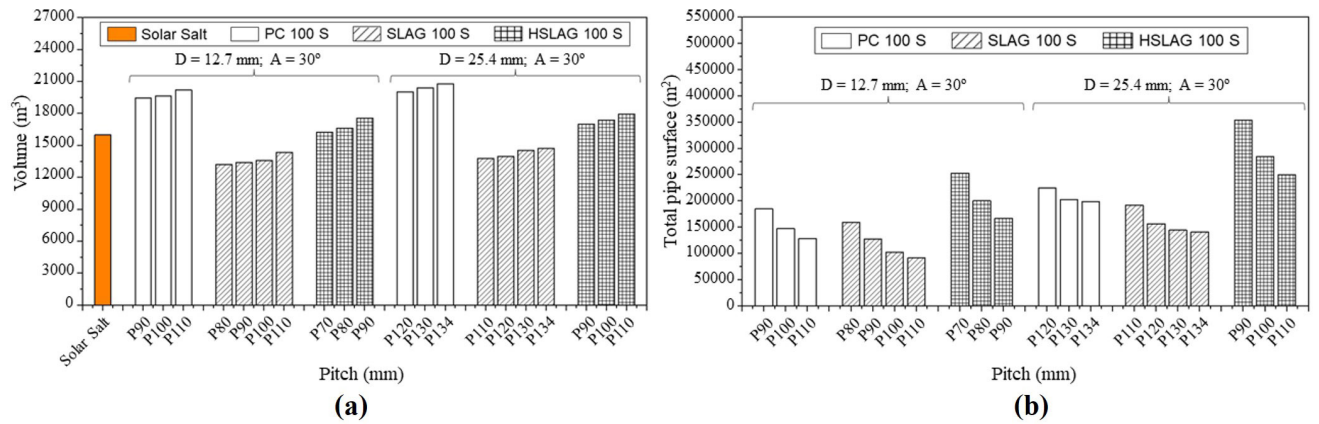

Figure 4: Volume required to store at least 1100 MWh (m^3) and **(b)** Total heat exchanger surface (m^2).

- SLAG 100S is the only mortar that can replace Solar Salt by decreasing the total volume without affecting the 1100 MWh of storage. Compared to the PC 100S, this alternative offers up to 3 different combinations that reduce both the total volume and the exchanger surface, which is the most expensive part of the TES block.

Acknowledgements

None.

Conflict of Interest

None.

References

1. Aarab F, Kuhn B, Bonk A, Bauer T. 2021. A new approach to low-cost, solar salt-resistant structural materials for concentrating solar power (CSP) and thermal energy storage (TES). *Metals* 11(12): 1970. https://doi.org/10.3390/met11121970
2. Alva G, Lin Y, Fang G. 2018. An overview of thermal energy storage systems. *Energy* 144: 341-378. https://doi.org/10.1016/j.energy.2017.12.037
3. Haider M, Werner A. 2013. An overview of state of the art and research in the fields of sensible, latent and thermo-chemical thermal energy storage. *Elektrotech Informationstech* 6(130): 153-160. https://doi.org/10.1007/s00502-013-0151-3
4. Hoivik N, Greiner C, Tirado EB, Barragan J, Bergan P, et al. 2017. Demonstration of EnergyNest thermal energy storage (TES) technology. *AIP Conf Proc* 1850(1): 080011. https://doi.org/10.1063/1.4984432
5. Laing D, Bahl C, Bauer T, Fiss M, Breidenbach N, et al. 2011. High-temperature solid-media thermal energy storage for solar thermal power plants. *Proc IEEE* 100(2): 516-524. https://doi.org/10.1109/JPROC.2011.2154290
6. Rao CR, Niyas H, Muthukumar P. 2018. Performance tests on lab–scale sensible heat storage prototypes. *Appl Therm Eng* 129: 953-967. https://doi.org/10.1016/j.applthermaleng.2017.10.085
7. Herrmann U, Kearney DW. 2002. Survey of thermal energy storage for parabolic trough power plants. *J Sol Energy Eng* 124(2): 145-152. https://doi.org/10.1115/1.1467601
8. Kumar R, Pathak AK, Kumar M, Patil AK. 2021. Experimental study of multi tubular sensible heat storage system fitted with wire coil inserts. *Renew Energy* 164: 1244-1253. https://doi.org/10.1016/j.renene.2020.10.058
9. Shabgard H, Bergman TL, Sharifi N, Faghri A. 2010. High temperature latent heat thermal energy storage using heat pipes. *Int J Heat Mass Transf* 53(15-16): 2979-2988. https://doi.org/10.1016/j.ijheatmasstransfer.2010.03.035
10. Tamme R, Laing D, Steinmann WD. 2004. Advanced thermal energy storage technology for parabolic trough. *J Sol Energy Eng* 126(2): 794-800. https://doi.org/10.1115/1.1687404
11. Selvam RP, Castro M. 2010. 3D FEM model to improve the heat transfer in concrete for thermal energy storage in solar power generation. *Energy Sustain* 43956: 699-707. https://doi.org/10.1115/ES2010-90078
12. Ramón-Álvarez I, Marugán-Cruz C, Enríquez E, Sánchez-Delgado S, Torres-Carrasco M. 2021. Alkali-activated and hybrid materials: alternative to Portland cement as a storage media for solar thermal energy. *Bol Soc Esp Ceram Vidr* 62(2): 160-173. https://doi.org/10.1016/j.bsecv.2021.11.006
13. Ramón-Álvarez I, Batuecas E, Sánchez-Delgado S, Torres-Carrasco M. 2023. Mechanical performance after high-temperature exposure and Life Cycle Assessment (LCA) according to unit of stored energy of alternative mortars to Portland cement. *Constr Build Mater* 365: 130082. https://doi.org/10.1016/j.conbuildmat.2022.130082
14. Shehata N, Sayed ET, Abdelkareem MA. 2021. Recent progress in environmentally friendly geopolymers: a review. *Sci Total Environ* 762: 143166. https://doi.org/10.1016/j.scitotenv.2020.143166
15. Feiz R, Ammenberg J, Baas L, Eklund M, Helgstrand A, et al. 2015. Improving the CO_2 performance of cement, part I: utilizing life-cycle assessment and key performance indicators to assess development within the cement industry. *J Clean Prod* 98: 272-281. https://doi.org/10.1016/j.jclepro.2014.01.083
16. Torres-Carrasco M, Puertas FJ. 2015. Waste glass in the geopolymer preparation. Mechanical and microstructural characterisation. *J Clean Prod* 90: 397-408. https://doi.org/10.1016/j.jclepro.2014.11.074
17. Garcia-Lodeiro I, Boudissa N, Fernández-Jiménez A, Palomo AJ. 2018. Use of clays in alkaline hybrid cement preparation. The role of bentonites. *Mater Lett* 233: 134-137. https://doi.org/10.1016/j.matlet.2018.08.098
18. Monteiro NB, Neto JM, da Silva EA. 2021. Environmental assessment in concrete industries. *J Clean Prod* 327: 129516. https://doi.org/10.1016/j.jclepro.2021.129516
19. Chaturvedy GK, Pandey UK. 2022. Performance characteristics of rubberized concrete: a multipoint review. *Innov Infrastruct Solut* 7: 1-18. https://doi.org/10.1007/s41062-021-00637-3
20. Fernández-Jiménez A, Garcia-Lodeiro I, Maltseva O, Palomo A. 2019. Hydration mechanisms of hybrid cements as a function of the way of addition of chemicals. *J Am Ceram Soc* 102(1): 427-436. https://doi.org/10.1111/jace.15939
21. Batuecas E, Ramón-Álvarez I, Sánchez-Delgado S, Torres-Carrasco M. 2021. Carbon footprint and water use of alkali-activated and hybrid cement mortars. *J Clean Prod* 319: 128653. https://doi.org/10.1016/j.jclepro.2021.128653
22. Zhang H, Baeyens J, Caceres G, Degreve J, Lv Y. 2016. Thermal energy storage: recent developments and practical aspects. *Prog Energy Combust Sci* 53: 1-40. https://doi.org/10.1016/j.pecs.2015.10.003
23. Boquera L, Castro JR, Pisello AL, Fabiani C, D'Alessandro A, et al. 2021. Thermal and mechanical performance of cement paste under high temperature thermal cycles. *Sol Energy Mater Sol Cells* 231: 111333. https://doi.org/10.1016/j.solmat.2021.111333
24. Kern DQ. 1950. Process Heat Transfer. McGraw-Hill, New York.
25. Ling TC, Poon CS, Wong HW. 2013. Management and recycling of waste glass in concrete products: current situations in Hong Kong. *Resour Conserv Recycl* 70: 25-31. https://doi.org/10.1016/j.resconrec.2012.10.006
26. de Castro S, de Brito J. 2013. Evaluation of the durability of concrete made with crushed glass aggregates. *J Clean Prod* 41: 7-14. https://doi.org/10.1016/j.jclepro.2012.09.021
27. Puertas F, Torres-Carrasco M. 2014. Use of glass waste as an activator in the preparation of alkali-activated slag. Mechanical strength and paste characterisation. *Cem Concr Res* 57: 95-104. https://doi.org/10.1016/j.cemconres.2013.12.005
28. Torres-Carrasco M, Puertas F. 2017. Waste glass as a precursor in alkaline activation: chemical process and hydration products. *Constr Build Mater* 139: 342-354. https://doi.org/10.1016/j.conbuildmat.2017.02.071
29. Kantarci F, Türkmen İ, Ekinci E. 2021. Improving elevated temperature performance of geopolymer concrete utilizing nano-silica, micro-silica and styrene-butadiene latex. *Constr Build Mater* 286: 122980. https://doi.org/10.1016/j.conbuildmat.2021.122980
30. Shoaib MM, Ahmed SA, Balaha MM. 2001. Effect of fire and cooling mode on the properties of slag mortars. *Cem Concr Res* 31(11): 1533-1538. https://doi.org/10.1016/S0008-8846(01)00561-0

31. Fernández-Jiménez A, Garcia-Lodeiro I, Maltseva O, Palomo A. 2019. Hydration mechanisms of hybrid cements as a function of the way of addition of chemicals. *J Am Ceram Soc* 102(1): 427-436. https://doi.org/10.1111/jace.15939

32. Luhar S, Nicolaides D, Luhar I. 2021. Fire resistance behaviour of geopolymer concrete: an overview. *Buildings* 11(3): 82. https://doi.org/10.3390/buildings11030082